PERGAMON

International Journal of Solids and Structures 37 (2000) 781–808

INTERNATIONAL JOURNAL OF SOLIDS and STRUCTURES

www.elsevier.com/locate/ijsolstr

The yield stress gradient effect in inhomogeneous materials

O. Kolednik [1]

Department for Materials Science and Engineering, Massachusetts Institute of Technology, 77 Massachusetts Avenue, Cambridge, MA 02139, USA

Received 22 September 1998; in revised form 5 March 1999

Abstract

In materials with local variations in yield stress, such as functionally graded materials or materials with interfaces or interlayers, the local near-tip crack driving force can become different from the nominally applied far-field value. The near-tip crack driving force is enhanced, if the yield stress increases in the crack growth direction, and vice versa. This effect is termed as the yield stress gradient effect. A model is developed that allows us to derive analytical expressions to quantify the effect and to evaluate the effective crack driving force for smooth and abrupt variations in yield stress. These expressions can be used to optimize graded materials and interface and interlayer transitions so that the fracture resistance increases. The predictions of the model agree well with the results of previously reported finite element computations for cracks near bimaterial interfaces. Available experimental observations of the fatigue crack growth normal to interfaces and interlayers can be qualitatively explained. The yield stress gradient effect plays an important role for the fracture behavior in multiphase or composite materials, in functionally graded materials, in materials with special surface treatments like nitrided or case hardened steels, as well as in brazed and welded components.

Keywords: Fracture toughness; Crack driving force; Interface; Interlayer; Functionally graded material; *J*-intergral

1. Introduction

1.1. The aim of this study

There exists a wide variety of applications in engineering practice where variations in yield stress appear, for instance, in welded structures, soldered joints, nitrided or case hardened components. In all structures consisting of multi-phase materials, composites, or graded materials, yield stress variations are inherent. A first experimental evidence that a gradient in yield stress influences the behavior of cracks

E-mail address: kolenik@unileoben.ac.at (O. Kolednik)

[1] On leave from the Erich Schmid Institute of Materials Science, Austrian Academy of Sciences, and the Institute of Metal Physics, University of Leoben, Jahnstraße 12, A-8700 Leoben, Austria.

0020-7683/00/$ - see front matter
PII: S0020-7683(99)00060-8

was found by Suresh et al. (1992) for fatigue cracks growing perpendicular to the interface of steel bimaterials. Later experiments, Suresh et al. (1993), further confirmed this finding and computational studies (Sugimura et al., 1995; Kim et al., 1997) have given a first hint to rationalize the observations.

The purpose of this paper is to provide an analytical model to explain why gradients in yield stress affect the crack growth behavior. It is demonstrated that a yield stress gradient induces an additional term of the crack driving force, which leads to an increase or decrease of the effective crack driving force. The predictions of the model are confirmed by available experimental observations and computational results. The model is applied to deduce the effective crack driving force for cracks near interfaces, at interlayers, in layered and in graded materials.

In the following, a brief survey of related literature will be given.

1.2. Background

1.2.1. Fracture mechanics studies

Numerous researchers have studied the fracture mechanics of inhomogeneous elastic materials. Classical papers dealing with cracks lying in a bimaterial interface are, for example, those by Williams (1959) and Rice (1988). An extensive overview of the behavior of interface cracks and of cracks parallel to interfaces has been given by Hutchinson and Suo (1992).

Cracks perpendicular to an interface have been analyzed, e.g., by Zak and Williams (1963), Cook and Erdogan (1972), Romeo and Ballarini (1995). The most relevant results are the following: When a crack lying in the elastically weaker material approaches the interface to a stiffer material, the (local) stress intensity decreases and reaches zero directly at the interface. For a crack in the stiffer material, the stress intensity increases to infinity at the interface. Chen et al. (1988) have studied the applicability of the J-integral for such crack geometries. Criteria for crack deflection at an interface were derived, among others, by He and Hutchinson (1989), Martinez and Gupta (1994) and Lee et al. (1996).

A comprehensive review of the processing and the properties of functionally graded materials (FGMs) has been presented recently by Suresh and Mortensen (1998). The fracture mechanics of cracks in FGMs has been developed in a series of papers by Erdogan and coworkers, e.g., Delale and Erdogan (1983), Erdogan (1995) and Erdogan and Wu (1997). It has been found that the stress intensity approach holds as long as the elastic properties remain piecewise continuous and differentiable. In general, the (local) stress intensity factor is higher than in a homogeneous material, if the Young's modulus, E, increases in crack growth direction, and vice versa. It is known that for cracks in gradient direction, the J-integral (Rice, 1968a, 1968b), becomes path dependent. Honein and Herrmann (1997) have derived an extension of the J-integral for FGMs which is path independent. Cracks near the boundary between a homogeneous material and an FGM have been considered by Delale and Erdogan (1988), Erdogan et al. (1991) and by Choi (1996). Numerical studies have been reported by Gu and Asaro (1997a, 1997b) and by Bao and Wang (1998).

Plasticity aspects have been taken into account in papers by Shih (1991), He et al. (1992), Delfin et al. (1995), Romeo and Ballarini (1997) and Wang and Ståhle (1998). These papers do not deal with the yield stress gradient effect but present small-scale yielding solutions for the stress and deformation fields of cracks at interfaces between materials with different elastic properties.

1.2.2. The yield stress gradient effect

Suresh et al. (1992) conducted fatigue experiments on an explosion clad bimaterial consisting of a ferritic and an austenitic steel. The elastic properties (Young's modulus, E, Poisson's ratio, υ) and the yield stresses, σ_y, of the two materials were approximately the same, but the strain hardening exponent, n, the tensile strength, σ_u, and the Vickers microhardness number, H, of the austenitic steel were significantly larger than those of the ferritic steel. The crack growth rate was measured for cracks perpendicular to

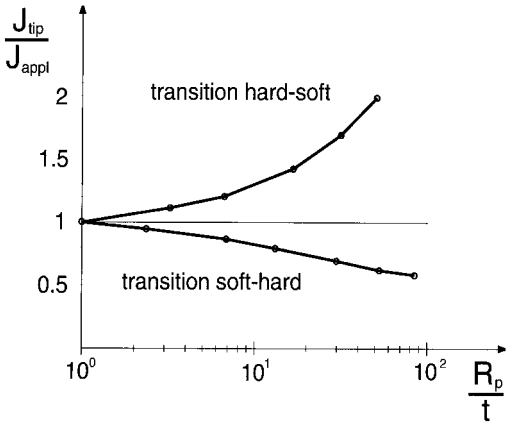

Fig. 1. A crack perpendicular to an interface between an elastic and an elastic–plastic material: the ratio of the near-tip J-integral, J_{tip}, to the far-field J-integral, J_{appl}, varies with the distance to the interface, t. R_p is the maximum extension of the plastic zone. From Sugimura et al. (1995).

the interface. The far-field stress intensity range, ΔK, was held constant throughout the test. For a crack approaching the interface from the softer ferritic steel (soft–hard transition), the crack growth rate dropped precipitously and the crack stopped some distance before the interface. On contrary, for a crack approaching the interface from the harder austenitic steel (hard–soft transition), the crack advanced through the interface. The crack growth rate remained roughly constant, except for some distance before the interface, where a slight increase of the crack growth rate was noted.

A practical application of this experimental finding has been reported in Suresh et al. (1993): The S–N curve (stress amplitude versus number of fatigue cycles to failure) of a steel coated with a 400 μm thick Cr_2O_3-layer is compared to that of a specimen that has a 50 μm thick soft Ni–5Al interlayer between steel and a Cr_2O_3-coating. The S–N curve of the specimen with the interlayer lies significantly above the curve of the specimen without the interlayer. The reasoning is that without the interlayer, the crack which is nucleated at the surface, grows unimpeded into the steel. The Ni–5Al interlayer, which is softer than the steel, provides a soft–hard transition at the second interface and hinders the promotion of the crack into the steel.

To rationalize the yield stress gradient effect, Sugimura et al. (1995) conducted finite element computations. They considered stationary, monotonically loaded cracks at various distances, t, from a bimaterial interface. The elastic constants are the same for both materials but the plastic properties differ. The loading was controlled by prescribing the remote stresses according to the elastic K-field solution. At given loadings, the near-tip J-integral, J_{tip}, is compared to the far-field J-integral, $J_{appl} = K^2(1-\nu^2)/E$ (for plane strain conditions). The results demonstrate that the near-tip crack driving force deviates from the far-field value when the crack approaches the interface. Fig. 1 gives an example, for an interface between a (plastically hard) elastic material and a (soft) elastic–plastic material with a yield stress, $\sigma_{y1} = 300$ MPa, and a strain-hardening exponent, $n = 1/N = 0.1$. The ratio J_{tip}/J_{appl} is plotted against R_p/t, with R_p as the maximum extension of the plastic zone in the soft material. The upper curve in Fig. 1 is for a hard–soft transition, i.e., the crack being in the elastic material; the near-tip crack driving force, J_{tip}, is higher than J_{appl}. The lower curve is for a soft–hard transition; J_{tip} lies below J_{appl}.

Kim et al. (1997) have compared the yield stress gradient effect in a bimaterial to those in a bimaterials with interlayers. Three cases are studied: 1. no interlayer, 2. a homogeneous interlayer with a con-

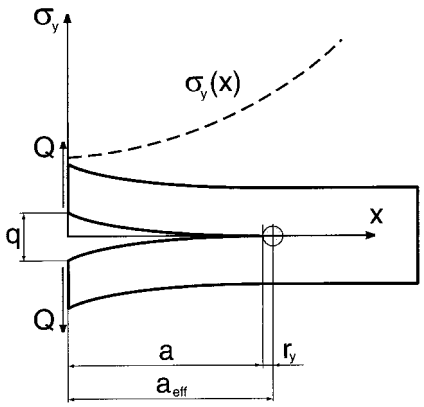

Fig. 2. Double Cantilever Beam specimen made of a non-linear material with a yield stress that has a gradient in the x-direction.

stant yield stress, $\sigma_{yi}=1/2(\sigma_{y1}+\sigma_{y2})$, 3. a graded interlayer with yield stresses between σ_{y1} and σ_{y2}. The yield stress gradient effect is found to be largest for Case 2 and smallest for Case 1, but the differences are not large.

2. An analytical model of the yield stress gradient effect

In this section, a model is presented to explain why in the example presented above the near-tip crack driving force differs from the far-field crack driving force when the crack approaches the interface.

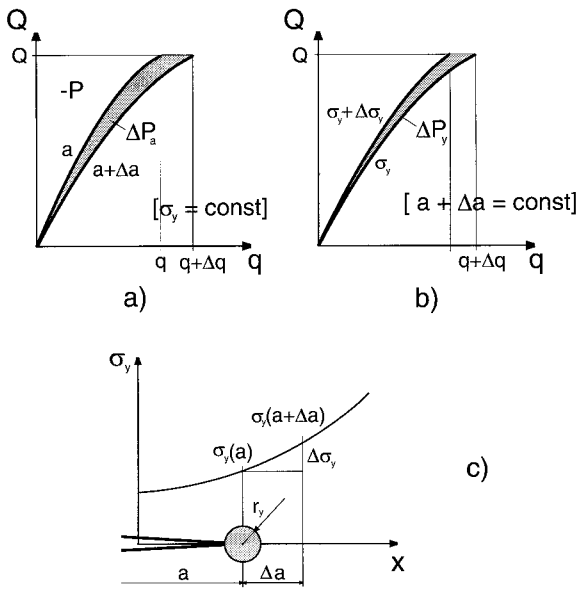

Fig. 3. (a) Change of the potential energy, ΔP_a, in a body during crack extension; the load, Q, and the yield stress, σ_y, are held constant. (b) Change of the potential energy, ΔP_y, due to an increase of the yield stress. (c) $\Delta P_a+\Delta P_y$ is the total change of the potential energy during crack extension in a body with a yield stress gradient in crack growth direction.

We consider a pre-cracked body of constant thickness, B, for example, a Double Cantilever Beam (DCB) specimen that is subjected to a pair of loads, Q, applying at the end points, Fig. 2. The body shall consist of a non-linear elastic material that has (during the loading) the same stress–strain response as an elastic–perfectly plastic material with a yield stress σ_y. The potential energy of an elastic body is given by (see Rice, 1968a):

$$P = \int_V \omega \, \mathrm{d}V - \int_{S_T} T_i u_i \, \mathrm{d}S, \tag{1}$$

where ω denotes the strain energy density which is integrated over the volume V. S_T is that portion of the total surface, S, where the traction vector, $\mathbf{T}$, is prescribed, and $\mathbf{u}$ is the displacement vector. As was pointed out by Rice (1968b), the potential energy for a load-controlled test, $P|_Q$, corresponds to the (negative) area above the load–displacement (Q–q) curve of the body [see Fig. 3(a)]:

$$P|_Q = -\int_0^Q q \, \mathrm{d}Q. \tag{2}$$

If the body were linear elastic, its potential energy would depend on the load, Q, the crack length, a, the Young's modulus, E, and the geometry of the body. (a, E, and the *geometry* of the body determine its compliance, ϕ). For our non-linear elastic body with the pseudo-yield stress, the potential energy depends additionally on σ_y:

$$P|_Q = P(Q, a, E, \mathit{geometry}, \sigma_y). \tag{3}$$

Note that at a given load, σ_y determines the radius of the pseudo-plastic zone, r_y, and, accordingly, the deviation of the Q–q curve from linearity. Throughout this paper, we assume that r_y is small against a and the specimen dimensions.

Now we conduct a thought experiment; the first part of which is well known:

1. We let the crack in the body advance by an increment, Δa, while the load, Q, σ_y, and the other parameters in Eq. (3), are held fixed. The potential energy of the body decreases by the amount ΔP_a, see Fig. 3(a). Rice (1968a) deduced that a certain line integral, the J-integral, is related to the potential energy change,

$$J = -\frac{1}{B}\frac{\partial P}{\partial a}\bigg|_Q, \tag{4}$$

   and that J is, thus, a measure of the crack driving force. The latter is true, however, only if the other three parameters in Eq. (3), E, *geometry* and σ_y, remain constant during the crack extension.
2. We let the yield stress increase by an increment, $\Delta\sigma_y$, while Q, a, E and *geometry* are held constant. The potential energy of our body will increase by the amount ΔP_y, see Fig. 3(b). Hence, if the yield stress of the body changes during crack extension, an additional term of the crack driving force will appear, given by

$$C_y = -\frac{1}{B}\frac{\partial P}{\partial \sigma_y}\bigg|_{Q,a}\frac{\mathrm{d}\sigma_y}{\mathrm{d}a}. \tag{5}$$

C_y is hereafter referred to as the yield stress gradient term. In a body with a gradient in yield stress in the direction of the crack growth, Fig. 3(c), the total change of the potential energy during crack extension is $\Delta P_a + \Delta P_y$. The total crack driving force, C_{tot}, is the sum of the terms in Eqs. (4) and (5):

$$C_{\mathrm{tot}} = -\frac{1}{B}\frac{\mathrm{d}P}{\mathrm{d}a}\bigg|_{Q,geometry} = J + C_{\mathrm{y}}. \tag{6}$$

The yield stress gradient term does not appear in a homogeneous body or in a body with a gradient in yield stress when the crack grows perpendicular to the gradient direction, because in both cases $\mathrm{d}\sigma_{\mathrm{y}}/\mathrm{d}a = 0$. Since $\partial P/\partial\sigma_{\mathrm{y}}|_{Q,a}$ is positive, the yield stress gradient term is negative if the yield stress increases in crack growth direction. The derivation of Eqs. (5) and (6) has been presented already in Kolednik and Suresh (1998)[2].

Irwin (1957) and Rice (1968a) demonstrated that the crack driving force is directly expressible in terms of deformations and stresses at the crack tip. Hence, there is a direct relation between the total crack driving force, C_{tot}, and the intensity of the crack tip field which can be determined by evaluating the line integral, J_{tip}, along a path close to the tip. This is the reason why Sugimura et al. (1995) found J_{tip}-values which are larger (for $C_{\mathrm{y}} > 0$) or smaller (for $C_{\mathrm{y}} < 0$) than the far-field J-integral, J_{appl}.

From the derivation in this section, it becomes clear that a similar effect can be expected, if a crack grows in the direction of a gradient in Young's modulus: Due to the occurrence of a modulus gradient term, C_E, the near-tip crack driving force differs from the applied far-field driving force, J_{appl}. It can be shown that for a Double Cantilever Beam specimen $J_{\mathrm{appl}} + C_E$ equals the new extension of the J-integral introduced by Honein and Herrmann (1997).

In the following section, the model will be applied to quantify the yield stress gradient effect in (functionally) graded materials, in materials with interfaces and interlayers, and in layered materials.

3. Applications of the model

3.1. Graded materials

A fracture mechanics specimen, for example, a double cantilever beam (DCB) specimen, shall consist of a material with a smooth yield stress gradient in the crack growth direction, Fig. 2. We consider the crack extension made in two steps, see Fig. 3: The first step is crack extension at a fixed loading for a constant yield stress; the crack driving force is given by J. The second step is to change the yield stress in the plastic zone according to the new tip position. To evaluate the total crack driving force, $C_{\mathrm{tot}} = J + C_{\mathrm{y}}$, an analytical expression for the potential energy, P, of the specimen is needed. This expression is then derived, first, with respect to the crack length to get the solution for J and, second, with respect to the yield stress to estimate C_{y}.

At a given load, Q,

$$q_{\mathrm{el}} = \frac{2}{3}\frac{Qa^3}{EI} \tag{7}$$

is the elastic component of the displacement. I denotes the moment of inertia of the cross-section of one beam. We assume, for small-scale yielding conditions, Irwin's model of a circular plastic zone at the crack tip, with its radius given by (Irwin, 1961)

$$r_{\mathrm{y}} = \beta\frac{GE}{\sigma_{\mathrm{y}}^2}. \tag{8}$$

[2] In Kolednik and Suresh (1998), C_{y} was denoted 'plasticity gradient term'; this nomenclature has been changed to 'yield stress gradient term' to avoid a possible confusion with effect of strain gradient plasticity.

σ_y is the yield stress at the center of the plastic zone. $\beta = 1/6\pi$ for plane strain conditions. G designates the elastic strain energy release rate which is, for the DCB-specimen,

$$G = \frac{Q^2 a^2}{BEI}. \tag{9}$$

A good estimate of the total displacement, $q_{tot} = q_{el} + q_{pl}$, is provided by replacing in Eq. (7) the crack length by the effective crack length, $a_{eff} = a + r_y$:

$$q_{tot} = \frac{2}{3}\frac{Qa_{eff}^3}{EI} = \frac{2}{3}\frac{Qa^3}{EI}\left(1 + \frac{r_y}{a}\right)^3. \tag{10}$$

The potential energy is calculated by substituting q_{tot} into Eq. (2) and integrating the area above the Q–q_{tot} curve. The result is

$$P = -\frac{1}{3}\frac{Q^2 a^3}{EI}\left(1 + \frac{3}{2}\frac{r_y}{a} + \left(\frac{r_y}{a}\right)^2 + \frac{1}{4}\left(\frac{r_y}{a}\right)^3\right). \tag{11}$$

Eq. (11), together with Eqs. (8) and (9), leads to the desired analytical expressions for J (by applying Eq. (4), C (applying Eq. (5)), and C_{tot} (applying Eq. (6)):

$$J = \frac{Q^2 a^2}{BEI}\left(1 + 2\frac{r_y}{a} + \frac{5}{3}\left(\frac{r_y}{a}\right)^2 + \frac{1}{2}\left(\frac{r_y}{a}\right)^3\right) \approx G\left(1 + 2\frac{r_y}{a}\right), \tag{12}$$

$$C_y = -\frac{Q^2 a^2}{BEI}\frac{r_y}{\sigma_y}\left(1 + \frac{4}{3}\frac{r_y}{a} + \frac{1}{2}\left(\frac{r_y}{a}\right)^2\right)\frac{d\sigma_y}{dx} \approx -J\frac{r_y}{\sigma_y}\frac{d\sigma_y}{dx} \tag{13}$$

$$C_{tot} \approx G\left(1 + 2\frac{r_y}{a} - \frac{r_y}{\sigma_y}\frac{d\sigma_y}{dx}\right) \approx J\left(1 - \frac{r_y}{\sigma_y}\frac{d\sigma_y}{dx}\right). \tag{14}$$

The right-hand side extensions of Eqs. (12)–(14) are first-order approximations. The difference between J and G is an analogue to the difference between K_{eff} and K. Eq. (13) states that the yield stress gradient term, C_y, is negative and the effective crack driving force is decreased, when the yield stress increases in crack growth direction. This is similar to the effect of a modulus gradient (Delale and Erdogan, 1983; Erdogan, 1995). The expression $\frac{r_y}{\sigma_y}\frac{d\sigma_y}{dx}$ can be seen as the relative variation of the yield stress within the radius of the plastic zone. A numerical example shall assess the order of magnitude of the yield stress gradient effect in FGMs: for $d\sigma_y/dx = 50$ MPa/mm, $\sigma_y = 500$ MPa, $r_y = 1$ mm, we get $C_y/J = -0.1$.

C_y can be evaluated in the way outlined above for any other geometry, where an analytical or power-series expression for the elastic compliance is known. In most cases, only the pre-factors within the parenthesis of Eq. (13) will be different. For a deeply notched bend specimen, however, the compliance depends on the ligament length, $\phi \sim b^{-2}$. Here, the second-order approximation of C_y becomes

$$C_y \approx -J\frac{r_y}{\sigma_y}\left(1 + \frac{r_y}{b}\right)\frac{d\sigma_y}{dx}. \tag{15}$$

The equation $C_y(x) = \text{const.}$, i.e., Eq. (13) with r_y substituted by Eq. (8), leads to a differential equation that can be solved to optimize the variation of $\sigma_y(x)$ in a functionally graded material.

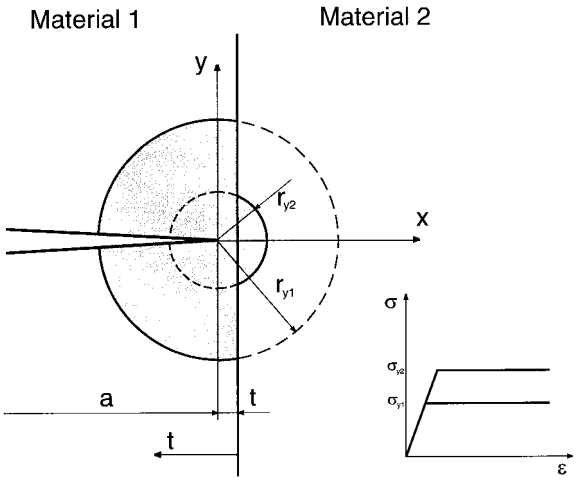

Fig. 4. The plastic zone of a crack near a bimaterial interface dividing Material 1 with yield stress σ_{y1} from Material 2 with yield stress σ_{y2}.

Adopting the boundary conditions $\sigma_y(0)=\sigma_{y0}$ and $\sigma_y(d)=\sigma_{yd}$, the solution becomes

$$\sigma_y(x)=\frac{\sigma_{y0}}{\sqrt{1-\frac{x}{d}\left[1-\left(\frac{\sigma_{y0}}{\sigma_{yd}}\right)^2\right]}}. \tag{16}$$

An example is depicted in Fig. 13. The corresponding size of the yield stress gradient term is given by

$$C_y \approx -\frac{\beta}{2}J\frac{r_{yd}}{d}\left[1-\left(\frac{\sigma_{y0}}{\sigma_{yd}}\right)^2\right]. \tag{17}$$

It should be stressed that the model presented in this section uses a constant yield stress for evaluating the plastic strain energy. The model should be applied only for cases where the relative variation of the yield stress within the plastic zone is small. The other limiting case is a sudden jump of the yield stress at an interface. This case is treated in the following section.

3.2. Cracks at bimaterial interfaces

In this section, an analytical expression for the yield stress gradient effect at a bimaterial interface is sought. The idea is the following: When the crack tip plastic zone is far from the interface, the plastic strain energy remains constant during an incremental crack extension (at a constant loading by a remote K-field) and the effective crack driving force is given by J. When the plastic zone touches the interface, an incremental crack extension produces a change in the total plastic strain energy of the body. Therefore, a yield stress gradient term appears, as in a graded material.

The procedure of the derivative is the following: First, the plastic zone model is introduced. Then, the plastic strain energy, W_{pl}, is determined for a plastic zone remote from the interface and for a plastic

zone intersecting the interface. Subsequently, the potential energy, and its total derivative, C_{tot}, can be evaluated for arbitrary crack tip locations.

We consider a bimaterial interface dividing Material 1, on the left-hand side, from Material 2 on its right-hand side. Both materials have an elastic–perfectly plastic response with identical elastic properties and with yield stresses σ_{y1} and σ_{y2}, respectively. A crack is located normal to the interface at a distance, t (Fig. 4). The body is loaded monotonically by remote stresses according to the elastic K-field solution.

Circular plastic zones are adopted. Their center is located at the crack tip and their radius, r_{y}, is given by Eq. (8). The plastic strain energy of the plastic zone is

$$W_{\mathrm{pl}} = B\int_0^{r_{\mathrm{y}}} \omega_{\mathrm{y}}(r) 2\pi r \, \mathrm{d}r. \tag{18}$$

The specific plastic strain energy per unit volume at a given radius, r, within the plastic zone shall have a r^{-1}-singularity of the form

$$\omega_{\mathrm{y}} = \frac{\gamma}{r}. \tag{19}$$

This type of singularity can be found in the HRR crack tip field solution (Hutchinson, 1968; Rice and Rosengren, 1968). The size of the constant, γ, is determined by equating W_{pl} given by Eq. (18) to the plastic work, that can be found by integrating the area below the load vs. plastic displacement curve (Q–q_{pl} curve). Again taken a DCB-specimen as an example, the integration yields (a first-order approximation is sufficient)

$$\gamma = \frac{3}{4\pi} G. \tag{20}$$

For other specimen geometries, the pre-factor in Eq. (20) can be slightly different. By inserting Eqs. (19) and (20) into Eq. (18), the plastic strain energy remote from the interface, $t > r_{\mathrm{y}}$ or $t < -r_{\mathrm{y}}$, is found:

$$W_{\mathrm{pl}} = \frac{3}{2} BGr_{\mathrm{y}} = \frac{3}{2}\beta B \frac{G^2 E}{\sigma_{\mathrm{y}}^2}. \tag{21}$$

Fig. 4 shows a plastic zone intersecting the interface for $r_{\mathrm{y2}} > t > -r_{\mathrm{y2}}$ and for $\sigma_{\mathrm{y2}} > \sigma_{\mathrm{y1}}$. The interface cuts off segments from the two plastic zones. The plastic strain energies in the two truncated plastic zones on either side of the interface can be integrated. The result is:

$$W_{\mathrm{pl1}}(t) = \begin{cases} \dfrac{3}{2} BGr_{\mathrm{y1}} & \text{for } t > r_{\mathrm{y1}} \\ \dfrac{3}{2\pi} BGr_{\mathrm{y1}} \left(\dfrac{1}{2}\pi + \arcsin\left(\dfrac{t}{r_{\mathrm{y1}}}\right) + \dfrac{t}{r_{\mathrm{y1}}} \operatorname{arctanh} \sqrt{1 - \left(\dfrac{t}{r_{\mathrm{y1}}}\right)^2} \right) & \text{for } r_{\mathrm{y1}} \geq t \geq -r_{\mathrm{y1}} \\ 0 & \text{for } t < -r_{\mathrm{y1}} \end{cases} \tag{22}$$

$$W_{\mathrm{pl2}}(t)=\begin{cases}0 & \text{for } t>r_{\mathrm{y2}}\\ \dfrac{3}{2\pi}BGr_{\mathrm{y2}}\left(\dfrac{1}{2}\pi-\arcsin\left(\dfrac{t}{r_{\mathrm{y2}}}\right)-\dfrac{t}{r_{\mathrm{y2}}}\operatorname{arctanh}\sqrt{1-\left(\dfrac{t}{r_{\mathrm{y2}}}\right)^2}\right) & \text{for } r_{\mathrm{y2}}\geq t\geq -r_{\mathrm{y2}}\\ \dfrac{3}{2}BGr_{\mathrm{y2}} & \text{for } t<-r_{\mathrm{y2}}\end{cases}. \tag{23}$$

The total plastic strain energy is the sum,

$$W_{\mathrm{pl}}(t)=W_{\mathrm{pl1}}(t)+W_{\mathrm{pl2}}(t). \tag{24}$$

The simplest way to derive an analytical expression for the potential energy, $P(t)$, is to use Eq. (21) for evaluating an effective total plastic zone radius,

$$\rho_{\mathrm{y}}(t)=\frac{2}{3}\frac{W_{\mathrm{pl}}(t)}{BG} \tag{25}$$

and substituting $\rho_{\mathrm{y}}(t)$ into Eq. (11). The partial derivative of $P(t)$ with respect to a leads to the J-integral. In analogy to Eq. (12),

$$J(t)\approx G\left(1+2\frac{\rho_{\mathrm{y}}(t)}{a}\right). \tag{26}$$

Since the potential energy is a function $P(t)=P(Q,a,E,\rho_{\mathrm{y}}(t))$, the yield stress gradient term is given by

$$C_{\mathrm{y}}(t)=-\frac{1}{B}\frac{\partial P}{\partial\rho_{\mathrm{y}}(t)}\frac{\mathrm{d}\rho_{\mathrm{y}}(t)}{\mathrm{d}t}\frac{\mathrm{d}t}{\mathrm{d}x}. \tag{27}$$

Note that $\mathrm{d}t/\mathrm{d}x=-1$. For convenience, the solution is split into two parts: $C_{\mathrm{y1}}(t)$ is the part that originates from the plastic zone in Material 1; $C_{\mathrm{y2}}(t)$ originates from the plastic zone in Material 2:

$$C_{\mathrm{y1}}(t)=\begin{cases}0 & \text{for } t>r_{\mathrm{y1}}\\ -\dfrac{G}{2\pi}\left(\operatorname{arctanh}\sqrt{1-\left(\dfrac{t}{r_{\mathrm{y1}}}\right)^2}\right) & \text{for } r_{\mathrm{y1}}\geq t\geq -r_{\mathrm{y1}}\\ 0 & \text{for } t<-r_{\mathrm{y1}}\end{cases} \tag{28}$$

$$C_{\mathrm{y2}}(t)=\begin{cases}0 & \text{for } t>r_{\mathrm{y2}}\\ \dfrac{G}{2\pi}\left(\operatorname{arctanh}\sqrt{1-\left(\dfrac{t}{r_{\mathrm{y2}}}\right)^2}\right) & \text{for } r_{\mathrm{y2}}\geq t\geq -r_{\mathrm{y2}}\\ 0 & \text{for } t<-r_{\mathrm{y2}}\end{cases}. \tag{29}$$

The total yield stress gradient term results as the superposition of the two partial components:

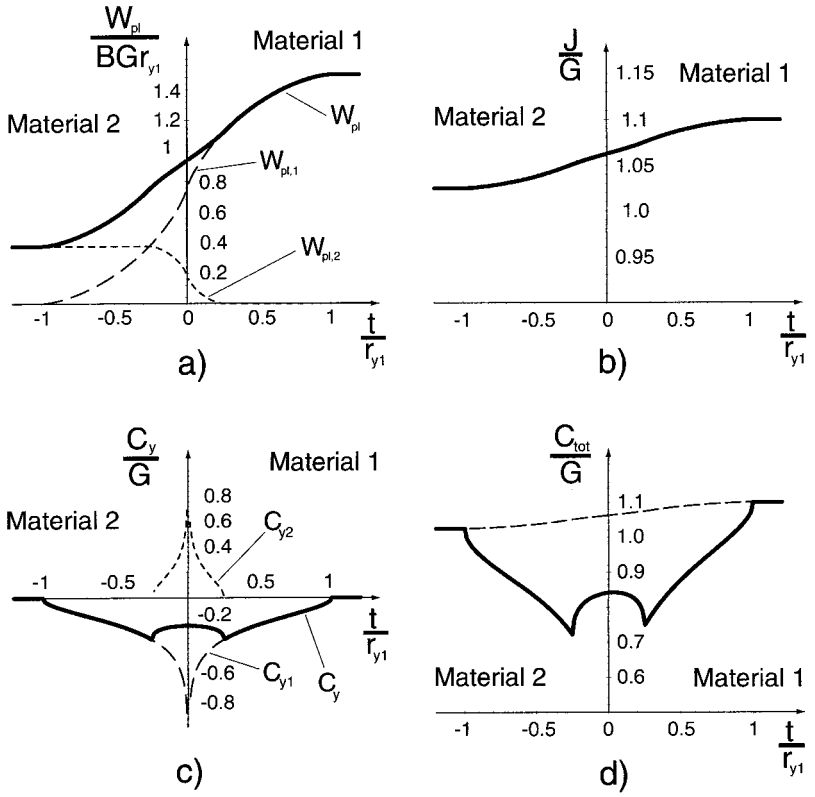

Fig. 5. A soft–hard transition at a bimaterial interface for $\sigma_{y2}=\sigma_{y1}/2$. (a) Variation of the plastic strain energy, W_{pl}, as a function of the distance of the crack tip from the interface, t. (b) The effective far-field J-integral, J. (c) The yield stress gradient term, C_y. (d) The total crack driving force, C_{tot}. B is the specimen thickness, G the applied strain energy release rate, and r_{y1} the plastic zone radius in Material 1.

$$C_y(t) = C_{y1}(t) + C_{y2}(t). \tag{30}$$

In Eqs. (26), (28) and (29) all but the first-order terms in $\rho_y(t)/a$ are neglected. For the exact solution, G should be replaced by

$$G\left(1+\frac{4}{3}\frac{\rho_y(t)}{a}+\frac{1}{2}\left(\frac{\rho_y(t)}{a}\right)^2\right).$$

$C_{y1}(t)$ describes the yield stress gradient term if Material 2 is elastic; the dashed line in Fig. 5(c) shows the maximum possible yield stress gradient effect for a given Material 1. The analogue is true for $C_{y2}(t)$ [dotted line in Fig. 5(c)]. To a first-order approximation, $C_{y1}(t)$ scales with G (or J). Apart from this, the functional value depends only on t/r_{y1}. That means that the width over which $C_{y1}(t)$ has a certain size, is a linear function of G and the plastic zone radius, r_{y1}. The singularities at $t = 0$ appear because the plastic strain energy density, ω_y, becomes infinite at the center of each plastic zone Eq. (19). The singularities could be avoided by introducing a maximum value of ω_y.

If both materials are elastic–plastic, the two singularities of opposite signs partly compensate and the resulting yield stress gradient term remains finite. For $r_{y1}=r_{y2}$, the two singularities cancel completely and $C_y(t)=0$. Fig. 5 presents a soft–hard transition for $\sigma_{y2}=2\sigma_{y1}$. During crack extension, the crack tip

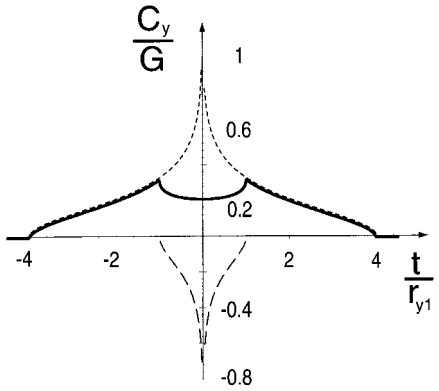

Fig. 6. A hard–soft transition at a bimaterial interface for $\sigma_{y2}=1/2\sigma_{y1}$. The yield stress gradient term, C_y, is positive and enhances the total crack driving force.

travels in each figure from the right-hand side to the left-hand side. Fig. 5(a) shows the variation of the plastic strain energy, W_{pl}; the curves of the partial terms, W_{pl1} and W_{pl2}, are also plotted. The effective far-field J-integral, the partial and total yield stress gradient terms, and the total crack driving force are plotted in Fig. 5(b,c,d). Fig. 5 demonstrates that a soft–hard transition with $\sigma_{y2}=2\sigma_{y1}$ produces a strong negative yield stress gradient term which reduces the total crack driving force by up to 33 percent.

Fig. 6 presents a hard–soft transition for $\sigma_{y2}=1/2\sigma_{y1}$. When the crack approaches the interface, $C_y(t)$ is positive and the total crack driving force is enhanced.

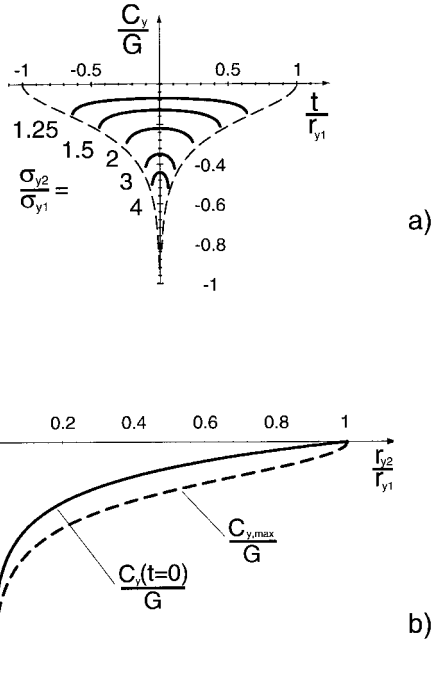

Fig. 7. A soft–hard interface transition: (a) Yield stress gradient term for different yield stress ratios. (b) Maximum yield stress gradient term, $C_{y,max}$, and yield stress gradient term at the interface, $C_y(t=0)$, as functions of the ratio of the plastic zone radii.

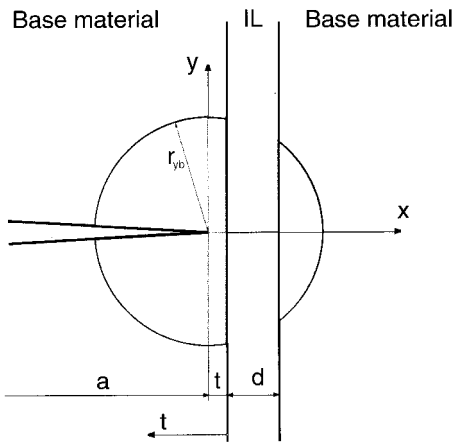

Fig. 8. Plastic zone of a crack near an elastic interlayer (IL) in an elastic–plastic base material.

Fig. 7(a) compares the yield stress gradient term for a soft–hard transition with fixed σ_{y1} and different yield stress ratios, σ_{y2}/σ_{y1}. The yield stress gradient term has its maximum,

$$|C_{y,max}| = \frac{G}{2\pi}\left(\operatorname{arctanh}\sqrt{1-\left(\frac{r_{y,hard}}{r_{y,soft}}\right)^2}\right), \tag{31}$$

at $t = \pm r_{y,hard}$. ($r_{y,hard}$ denotes the plastic zone radius of the harder material). The evaluation of C_y at the position of the interface yields

$$C_y(t=0) = \frac{G}{2\pi}\ln\left(\frac{r_{y2}}{r_{y1}}\right). \tag{32}$$

Fig. 7(b) can be used to estimate the maximum size of the yield stress gradient term for a given bimaterial combination: $C_{y,max}$ and $C_y(t = 0)$ are drawn against the ratio of the plastic zone radii.

The analogy between the yield stress gradient effect and the effect of a modulus gradient at an interface is obvious: a soft–hard transition of either the yield stress or the Young's modulus leads to a decrease of the effective crack driving force; a hard–soft transition increases C_{tot}.

3.3. The yield stress gradient effect at interlayers

3.3.1. Elastic interlayer in elastic–plastic base material

First we consider the effect of an elastic interlayer of thickness d in an elastic–plastic material (Fig. 8). σ_{yb} is the yield stress and r_{yb} the plastic zone radius of the base material. The interlayer cuts off a strip of width d from the plastic zone. The plastic strain energy of the material on the left-hand side of the interface is given by Eq. (22), with r_{yb} inserted instead of r_{y1}. The plastic strain energy on the right-hand side of the interlayer is found by replacing r_{y2} and t in Eq. (23) with r_{yb} and $(t+d)$. The yield stress gradient term becomes

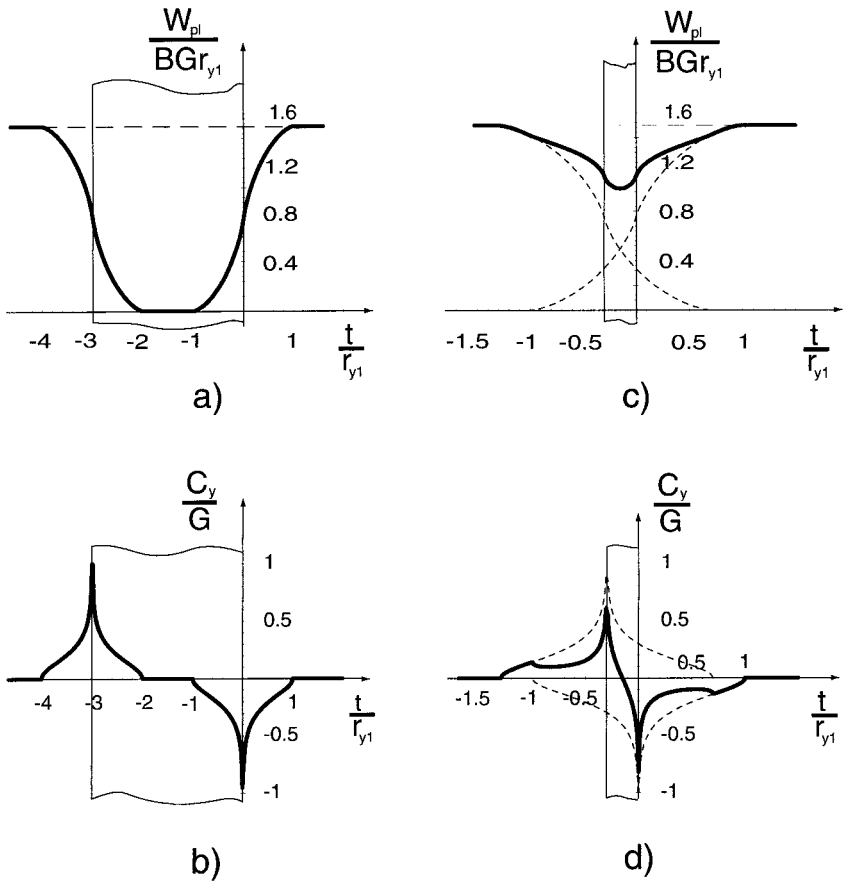

Fig. 9. Elastic interlayer in an elastic–plastic base material. (a) Variation of the plastic strain energy, W_{pl}, and (b) of the yield stress gradient term, C_{y}, for a thick interlayer. (c,d) Variation of W_{pl}, and C_{y} for a thin interlayer. The minimum crack driving force appears at the first interface.

$$C_{\mathrm{yb}}(t)=\begin{cases}0 & \text{for } t > r_{\mathrm{yb}}\\ -\dfrac{G}{2\pi}\left(\operatorname{arctanh}\sqrt{1-\left(\dfrac{t}{r_{\mathrm{yb}}}\right)^2}\right) & \text{for } r_{\mathrm{yb}}\geq t > r_{\mathrm{yb}}-d\\ -\dfrac{G}{2\pi}\left(\operatorname{arctanh}\sqrt{1-\left(\dfrac{t}{r_{\mathrm{yb}}}\right)^2}-\operatorname{arctanh}\sqrt{1-\left(\dfrac{t+d}{r_{\mathrm{yb}}}\right)^2}\right) & \text{for } r_{\mathrm{yb}}-d\geq t > -r_{\mathrm{yb}}\\ \dfrac{G}{2\pi}\left(\operatorname{arctanh}\sqrt{1-\left(\dfrac{t+d}{r_{\mathrm{yb}}}\right)^2}\right) & \text{for } -r_{\mathrm{yb}}\geq t > -d-r_{\mathrm{yb}}\\ 0 & \text{for } t\leq q-d-r_{\mathrm{yb}}\end{cases}. \tag{33}$$

In Fig. 9, the variation of the plastic strain energy and the yield stress gradient term is drawn for two different d/r_{yb}-ratios. The C_{yb}–t curve shows two opposite singularities of equal size appearing at $t = 0$

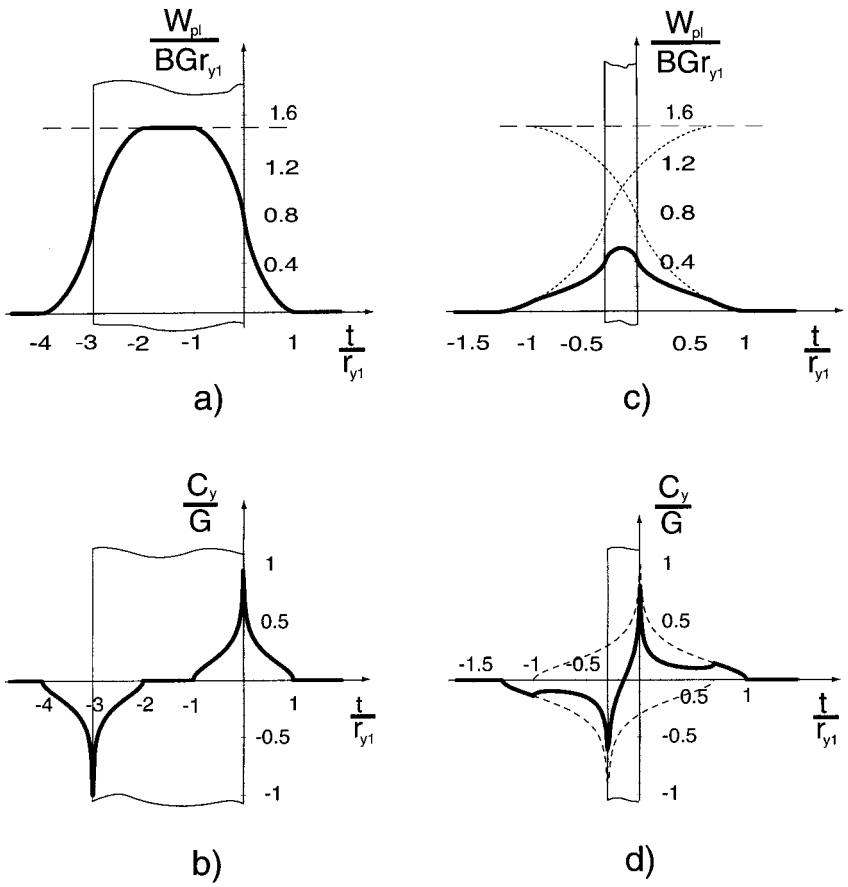

Fig. 10. Elastic–plastic interlayer in an elastic base material. (a) Variation of the plastic strain energy, W_{pl}, and (b) of the yield stress gradient term, C_y, for a thick interlayer. (c,d) Variation of W_{pl}, and C_y for a thin interlayer. The minimum crack driving force appears at the second interface.

and $t=-d$. The yield stress gradient term is negative when the crack approaches the first interface; C_y is positive near the second interface. For thick interlayers, $d/r_{yb} \geq 2$, the effect of the interlayer is that of two consecutive interfaces. For thin interlayers, the two C_y-peaks come close and interfere. The yield stress gradient effect increases with increasing d/r_{yb}-ratio, but only up to $d/r_{yb} \approx 1$. No significant enhancement is observed for thicker interlayers. For $d/r_{yb} \geq 1$, Eq. (31) or Eq. (32) can be used to estimate the maximum size of the yield stress gradient term.

3.3.2. Elastic–plastic interlayer in elastic base material

The other limiting case is that of an elastic–plastic interlayer (thickness d, yield stress σ_{yL}, plastic zone radius r_{yL}) in an elastic matrix. The solution is similar to that of the foregoing case; however, the sign of the effect is different: The first interface attracts the crack, the second interface repels the crack. The equations are:

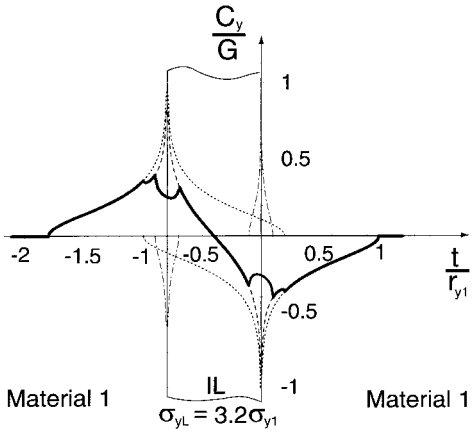

Fig. 11. Variation of the yield stress gradient term, C_y, for a hard interlayer in a soft base material. The minimum crack driving force appears near the first interface.

$$C_{yL}(t)=\begin{cases}0 & \text{for } t > r_{yL}\\ \dfrac{G}{2\pi}\left(\operatorname{arctanh}\sqrt{1-\left(\dfrac{t}{r_{yL}}\right)^2}\right) & \text{for } r_{yL}\geq t > r_{yL}-d\\ \dfrac{G}{2\pi}\left(\operatorname{arctanh}\sqrt{1-\left(\dfrac{t}{r_{yL}}\right)^2}-\operatorname{arctanh}\sqrt{1-\left(\dfrac{t+d}{r_{yL}}\right)^2}\right) & \text{for } r_{yb}-d\geq t > -r_{yb}\\ -\dfrac{G}{2\pi}\left(\operatorname{arctanh}\sqrt{1-\left(\dfrac{t+d}{r_{yL}}\right)^2}\right) & \text{for } -r_{yb}\geq t > -d-r_{yb}\\ 0 & \text{for } t\leq q-d-r_{yb}\end{cases} \quad . \tag{34}$$

Fig. 10 collects W_{pl}–t and C_{yL}–t curves for two d/r_{yL}-ratios. Again, the maximum size of the yield stress gradient term increases with increasing d/r_{yL}, but not beyond $d/r_{yb}=1$.

3.3.3. The general case

In general, both the base material and the interlayer deform plastically. The solution for the yield stress gradient term can be easily found as the superposition of the preceding two limiting cases:

$$C_y(t)=C_{yb}(t)+C_{yL}(t) \tag{35}$$

One example is presented in Fig. 11, for a hard interlayer in a soft matrix: $r_{yL}/r_{yb}=1/10$, $d/r_{yL}=0.8$. The curve is similar to the case of the elastic interlayer, but the two opposite singularities are truncated because of the plasticity of the interlayer. The interlayer thickness is not yet optimal; the maximum yield stress gradient term would be somewhat larger, if the interface were thicker.

We have seen that both hard and soft interlayers produce a region of negative yield stress gradient term. This region lies near the first interface for a hard interlayer, near the second interface for a soft interlayer. The size of the yield stress gradient term depends primarily on the yield stress ratio and the ratio of the plastic zone radius of the softer material versus the interlayer thickness. For a large effect, the latter ratio should be 1 or higher.

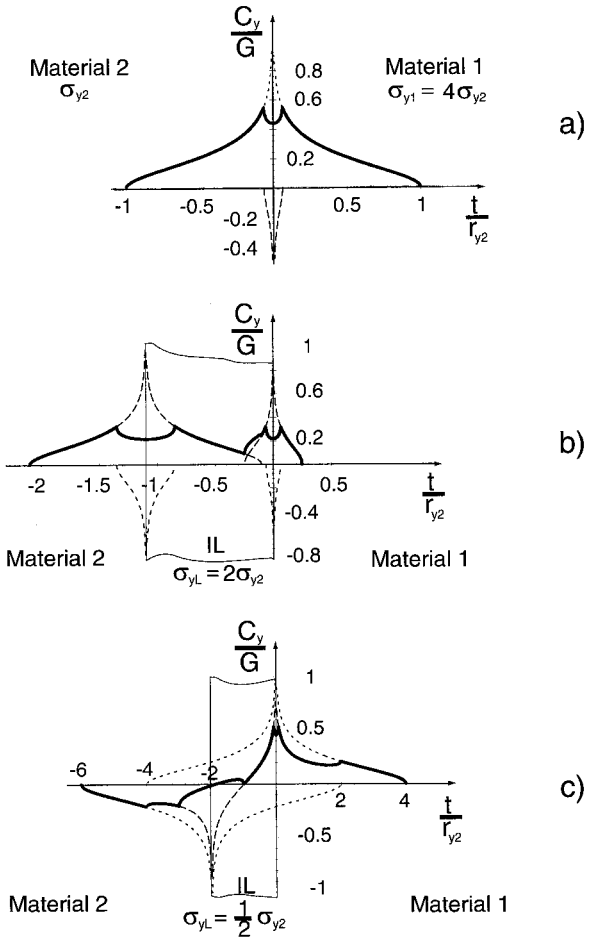

Fig. 12. (a) A high, positive yield stress gradient term, C_y, appears at a bimaterial transition from a hard surface layer to a soft base material. (b) An interlayer with an intermediate yield stress reduces the maximum value of C_y. (c) Behind an interlayer that is softer than the base material, a beneficial zone of negative C_y appears.

3.3.4. Interlayers at a bimaterial boundary

The previous sections have dealt with interlayers lying within one type of base material. In a vast number of technical applications, a hard surface layer protects a softer base material ($\sigma_{y,hard} \gg \sigma_{y,soft}$). If the surface layer contains a crack, a large positive yield stress gradient term will appear. The following questions should be answered in this section: Can interlayers between surface layer and base material reduce the total crack driving force? What are the optimum yield stress and the optimum thickness of such interlayers?

First we consider a single interlayer. The question about the optimum yield stress, σ_{yL}, of the interlayer can be answered immediately: The maximum yield stress gradient term at an interface depends on the ratio of the plastic zones, Eq. (32) and hence, on the ratio of the yield stresses. Accordingly, the yield stress of the interlayer must be the geometric mean value of the bimaterial yield stresses, $\sigma_{yL} = \sqrt{\sigma_{y,hard}\sigma_{y,soft}}$, to guarantee that the yield stress gradient terms at both interfaces are equal in size. With σ_{yL} known, the C_y–t curves can be drawn and arranged for arbitrary interlayer thicknesses, d. If d is

Table 1
Bimaterial transition between a hard surface and a soft base material for $\sigma_{y1}/\sigma_{y2}=4$: the maximum yield stress gradient term, $C_{y,max}$, decreases with increasing numbers of layers, n; the optimum total width of the transition zone, σd_i, increases. (G is the applied strain energy release rate and r_{y2} the plastic zone radius in the base material)

n	0	1	2	3	4	5	6	7	8
$C_{y,max}/G$	0.55	0.33	0.25	0.21	0.18	0.165	0.15	0.14	0.13
$\frac{1}{r_{y2}}\sum_{i=1}^{n} d_i$	0	1.06	1.62	2.19	2.71	3.41	4.03	4.77	5.32

smaller than the plastic zone radius of the soft base material, $r_{y,soft}$, the interlayer brings no relief; $C_{y,max}$ may be even larger than without interlayer. However, the yield stress gradient term is reduced significantly, if $d \geq (r_{y,soft}+r_{y,hard})$. To present an example, Fig. 12(a) depicts a bimaterial transition for $\sigma_{y,hard}=4\sigma_{y,soft}$ without interlayer; the maximum yield stress gradient term amounts $C_{y,max}/G = 0.55$. Fig. 12(b) shows the situation with an interlayer having $\sigma_{yL}=2\sigma_{y,soft}$, $d=r_{y,soft}+r_{y,hard}$. Compared to the situation without interlayer, the yield stress gradient term decreases by 40 percent, $C_{y,max}/G = 0.33$.

The maximum yield stress gradient term can be further reduced, if several interlayers are inserted between surface layer and base material; however, it must be guaranteed that each interlayer is thick enough. From the preceding paragraph it can be deduced that the thickness of each layer should be at least the sum of the plastic zone radii of the two neighboring layers. The following equations, which have been presented already in Kolednik and Suresh (1998), give the optimum yield stress, σ_{yL}^{i}, and thickness, d_i, of the ith interlayer, if n interlayers between hard and soft material have been introduced:

$$\sigma_{yL}^{i} = \sigma_{y,hard}\left(\frac{\sigma_{y,soft}}{\sigma_{y,hard}}\right)^{\frac{i}{n+1}} \tag{36}$$

and

$$d_i = r_{y,hard}\left(\frac{\sigma_{y,hard}}{\sigma_{y,soft}}\right)^{2\frac{i-1}{n+1}}\left[1+\left(\frac{\sigma_{y,hard}}{\sigma_{y,soft}}\right)^{\frac{4}{n+1}}\right]. \tag{37}$$

If the conditions of Eqs. (36) and (37) are met, the maximum yield stress gradient term is

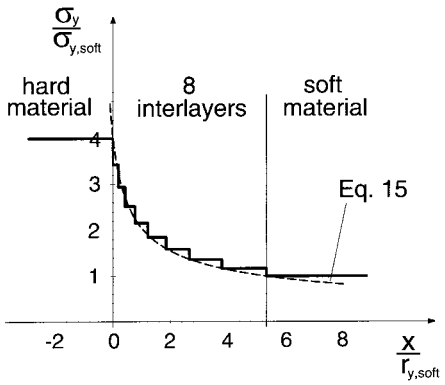

Fig. 13. Optimum transition between a hard surface layer and a soft base material consisting of 8 interlayers; $C_{y,max}=0.13G$. The dashed line indicates a smooth yield stress gradient with $C_y=0.08G$.

$$|C_{y,max}| = \frac{G}{2\pi}\operatorname{arctanh}\sqrt{1-\left(\frac{\sigma_{y,soft}}{\sigma_{y,hard}}\right)^{\frac{4}{n+1}}} \tag{38}$$

Eqs. (36) and (37) allow the design of optimum bimaterial transitions. Table 1 lists for $\sigma_{y,hard}=4\sigma_{y,soft}$ the maximum size of the yield stress gradient term, $C_{y,max}/G$, and the total interlayer thickness related to the plastic zone radius of the soft base material, $\frac{1}{r_{y,soft}}\sum_{i=1}^{n} d_i$, as a function of the number of interlayers, n. Fig. 13 presents, as an example, the optimum yield stress variation for 8 interlayers. The solution of the differential equation for a smooth transition, Eq. (16) is indicated as a dashed line. It is noteworthy that the smooth transition would yield $C_y/G \approx 0.08$, compared to the $C_{y,max}/G = 0.13$ for the 8 interlayers with abrupt changes in σ_y.

Very interesting is the case of a single interlayer which is softer than the base material. Fig. 12(c) presents the situation for $\sigma_{yL}=\sigma_{y,soft}/2$, $d=r_{yL}/2=2r_{y,soft}$. At the first interface, C_y is almost the same as for the case without interlayer, but behind the second interface a zone of negative C_y appears which reduces the propensity of the crack to grow deeper into the base material. Note that the interlayer must be thick enough to be effective: the interlayer depicted in Fig. 12(c) is too small; the optimum thickness is $d=r_{yL}$. The benefit of such a soft interlayer has been shown experimentally by Suresh et al. (1993) for a Cr_2O_3-coated steel with a Ni–5Al interlayer, see Section 1.2.2.

3.4. Layered materials

Consider a layered material consisting of two phases; r_{y1} and r_{y2} are the plastic zone sizes and d_1 and d_2 the layer thicknesses. If the plastic zone radius of the softer phase, $r_{y,max}$, is much larger then both the periodicity of the material, d_1+d_2, and the minimum layer thickness (of either the soft or the hard phase), d_{min}, the yield stress gradient effect will be negligible. On the contrary, a significant effect will appear, if the maximum plastic zone radius has the same order of magnitude as the minimum layer thickness. For $2r_{y,max} \le d_{min}$, the situation resembles those in two alternative bimaterial interfaces; $C_y(t)$ is evaluated with Eqs. (28) and (29). For other cases, the equations which have been developed in Section 3.3 can be combined to deduce the variation of the yield stress gradient term.

4. Discussion

4.1. Some remarks on the applied model

In the previous section, a simple energetically-based model has been developed to evaluate the yield stress gradient term for materials with smooth and abrupt variations in yield stress. The advantage of the model is that it provides analytical expressions of the yield stress gradient term which are useful for the optimization of structural components with respect to their fracture properties.

The model has a few deficiencies. The first deficiency is that it does not allow for the strain hardening of materials. It is clear that a yield stress gradient term will be induced also on an interface of two materials with equal yield stresses but different strain hardening exponents. It should be possible to adapt the model for power-law hardening materials, e.g., by applying the EPRI-approach, Kumar et al. (1981), but this has not been done yet. An engineering approximation to assess the yield stress gradient term would be to insert into the equations an average flow stress, $\bar{\sigma}_{flow}$, instead of the yield stress. Unless a more sophisticated solution is known, the mean value between the yield stress and the ultimate tensile strength, σ_u, could serve as a rough estimate for $\bar{\sigma}_{flow}$.

A second shortcoming of the model is that it assumes a circular plastic zone with its center at the

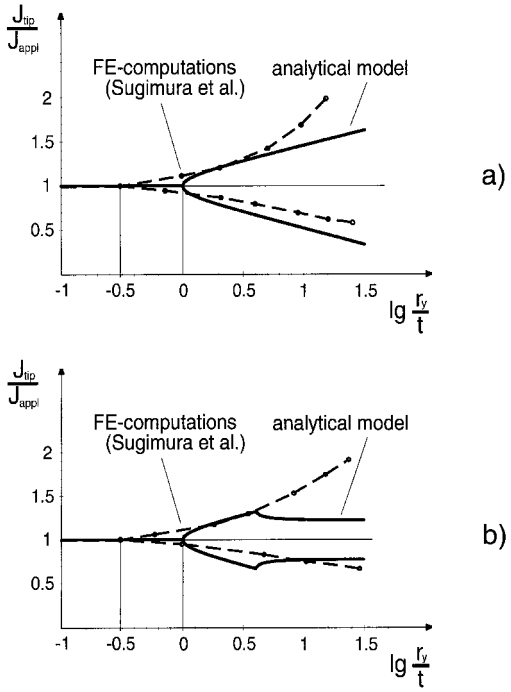

Fig. 14. Comparison between the predictions of the current analytical model and finite element computations by Sugimura et al. (1995) for bimaterial transitions. The ratio of the near-tip J-integral to the applied far-field J-integral, J_{tip}/J_{appl}, is plotted against the plastic zone radius in the softer material related by the distance to the interface, r_y/t. (a) The harder material is elastic. (b) The harder material has twice the yield stress of the softer material.

crack tip. In reality, the plastic zone has a more complicated shape with a forward orientation, i.e., it extends much farther towards the crack growth (positive x-) direction. The consequence is that the $C_y(t)$-curve for a crack approaching a bimaterial interface, e.g., Fig. 5(c), becomes non-symmetrical with respect to the interface: the branches of the curves for positive t will be longer than those for negative t, see also Section 4.2.

It should be also remarked that the model does not consider misfit strains which will appear when the plastic zone intersects the interface between materials with different yield stresses. It is expected that the effect of such misfit strains on the yield stress gradient effect will not be large: they will tend to decrease the plastic zone size near the interface on the softer side, and increase it on the harder side; however, the sum of the plastic strain energy will not change a lot.

4.2. Comparison to finite element solutions

Fig. 14 compares the predictions of the current analytical model to the results of the finite element (FE) computations by Sugimura et al. (1995), see Section 1.2.2. It might be interesting that the computations were made using both a J_2 deformation theory of plasticity and a J_2 (rate independent) flow theory of plasticity with isotropic hardening ($N = 10$). For J_{tip} the two theories yielded identical solutions, for remote paths the solutions differed only by 2% or less. Fig. 14(a) considers a bimaterial interface between an elastic material and an elastic–plastic material with a yield stress, σ_y. The ordinate of the diagram scales the ratio of the near-tip J-integral to the far-field J-integral, J_{tip}/J_{appl}, which is equivalent to the ratio C_{tot}/J. The abscissa measures the plastic zone radius in the softer material related by the dis-

tance to the interface, r_y/t, drawn in a logarithmic scale (base 10). According to the analytical model (solid line), J_{tip} equals J_{appl} up to the point $\lg\frac{r_y}{t} = 0$, where the plastic zone touches the interface. Then the curve bifurcates: the lower curve pertains to the transition soft–hard, when the crack lies in the elastic–plastic material; the upper curve pertains to the transition hard–soft. In the FE model (dashed line), the yield stress gradient effect is initiated at larger distances from the interface because the actual maximum extension of the plastic zone in the crack growth direction, R_{px}, is larger than the plastic zone radius, r_y, given by the Irwin model. Sugimura et al. (1995) have reported that the plastic zone reaches the interface at $\frac{K}{\sigma_y\sqrt{t}} = 2.5$; accordingly, $R_{px} = 3.0r_y$).

For the hard–soft transition, the results of the analytical model and the FE model agree very well. The predictions of the two models begin to deviate when the plastic zone size becomes large. The reason might be the small-scale yielding assumption of the analytical model. For the soft–hard transition, the FE model predicts a smaller yield stress gradient effect than the analytical model. In both models, J_{tip} shows a singularity at the interface, i.e., for $r_y/t \to \infty$.

If the harder material is not elastic, but has twice the yield stress of the softer material [Fig. 14(b)], the analytical model yields the same J_{tip}/J_{appl}-curves up to $\lg\frac{r_y}{t} = \lg 4 = 0.60$, where C_y reaches its maximum [see Fig. 5(c)]. For higher r_y/t-values, J_{tip}/J_{appl} decreases slightly and attains a constant value towards the interface. The FE solution is similar to those for the case with the harder material being elastic. Again, the curves indicate singularities of J_{tip} at the interface. For real elastic–plastic materials, such singular J_{tip}-values are unrealistic.

The major difference between the analytical model and the FE model is that the analytical model produces symmetric effects in the respect whether the crack is located either in the harder or the softer material; the FE model not. The reason is that when a crack propagates within the softer material, its plastic zone does not simply translate with the crack tip, but it also changes its shape in front of an interface. Thus, the actual change of the plastic energy is a little bit less than predicted by a simple translation model, and the yield stress gradient term is overestimated.

In summary, it can be stated that the two models fit well as long as the ratio r_y/t does not become too high. The analytical model becomes inaccurate when the conditions of small-scale yielding are not met. The FE model fails in yielding reasonable estimates for the maximum or minimum near-tip crack driving forces at interfaces.

4.3. Crack driving force and fracture toughness

The behavior of a crack within a (plastically) inhomogeneous body depends on the ratio between the local crack driving force and the local crack growth resistance: the crack extends if the local crack driving force equals or exceeds the crack growth resistance. We have seen that, given a constant applied crack driving force, the near-tip crack driving force, C_{tot}, varies significantly with the distance of the crack tip from an interface, t. The local crack growth resistance will also vary, but probably in a different manner. Hence, we do, per se, not know how the local fracture properties of a body vary near a bimaterial interface.

A definite answer to this question would require experiments where the local fracture initiation toughness and the local crack growth toughness are determined as a function of the distance, t. This could be done by measuring COD_i and the crack tip opening angle, $CTOA$, by stereoscopic analyses and the application of a new digital image analysis system (Stampfl et al., 1996; Stampfl and Kolednik, 1998). Such data are not available now; however, we can try to guess a preliminary answer:

Imagine a crack at some distance from an interface dividing a low-strength from a high-strength material. We measure the crack driving force in terms of the crack tip opening displacement, COD, and the fracture initiation toughness in terms of the critical crack tip opening displacement, COD_i.

C_{tot}, which corresponds to the near-tip J-integral, J_{tip}, determines the stresses and deformations within

Table 2
Influence of the T-stress on the plastic zone size; λ gives the ratio of the plastic zone size relative to those for $T = 0$

T/σ_y	−0.75	−0.5	0	0.5	0.75
$R_p \frac{\sigma_y^2}{GE}$	0.88	0.35	0.15	0.13	0.24
λ	5.9	2.3	1	0.87	1.6

the local crack tip field and, hence, also the crack tip opening displacement, COD. As soon as the plastic zone touches the interface, COD will begin to decrease. Pippan and co-workers estimated the variation of COD for cracks near interfaces (Pippan and Riemelmoser, 1999) and at interlayers (Pippan et al., 1998), applying a Dugdale model.

The crack growth resistance of a material depends primarily on the conditions that prevail within the process zone directly ahead of the blunted crack tip. These conditions determine either the microstructural processes, void nucleation, growth, and coalescence, of a microductile fracture, or the attainment of a critical normal stress for a cleavage fracture.

Since the size of the process zone is one order of magnitude smaller than the plastic zone, we expect that COD_i remains constant as long as the process zone is far from the interface, $r_y \geq t \gg l_{pz}$. As the driving force, COD, decreases when the crack approaches the interface, we notice a real improvement of the fracture properties: the material in front of a soft–hard transition behaves tougher.

4.4. Influences of the stress state and the T-stresses

Larsson and Carlsson (1973) and Rice (1974) have found that even for small-scale yielding conditions the size of the plastic zone is influenced by the size of the second (r^0-) term of the asymptotic stress field solution for a sharp crack in an elastic material. These stresses, called T-stresses, are non-negative for high-constraint situations, such as in deeply notched bend or Compact Tension specimens. Large negative T-stresses occur in specimens with shallow cracks or, e.g., in Center Cracked Tension specimens.

Both the stress state and the T-stresses affect the plastic zone size and the plastic strain energy and, accordingly, the yield stress gradient term. Their influence can be easily assessed for with our model:

The stress state can be allowed for by adjusting the constant β in Eq. (8) from $\beta = 1/6\pi$ for plane strain conditions to $\beta = 1/2\pi$ for plane stress conditions. The effect of the T-stresses can be estimated by introducing a T-stress dependent pre-factor, λ, into the equation of the plastic zone radius:

$$r_y = \lambda\left(\frac{T}{\sigma_y}\right)\beta\frac{GE}{\sigma_y^2}. \tag{39}$$

Rice (1974) has derived a model to estimate the maximum size of the plastic zone, R_p, for different T/σ_y-values; in Sugimura et al. (1995) R_p-values have been tabulated for a strain hardening exponent, $n = 1/N = 0.1$. From this table, λ-values can be generated, bearing in mind that $\lambda(0) = 1$ and that for $T = 0$ the plastic zone size must be twice the plastic zone radius, $R_p = 2r_y$. Table 2 lists λ-values for different T/σ_y-ratios.

Negative T-stresses, as well as plane stress conditions instead of plane strain conditions, enhance the yield stress gradient term in a material with a smooth yield stress gradient, see Eq. (13). At interfaces, negative T-stresses increase the regions over which a certain yield stress gradient term prevails because they increase the plastic zone radius; however, they do not enhance the maximum yield stress gradient term, see Eqs. (26) and (28). At interlayers, the effect of the T-stresses depends on the ratio of the interlayer thickness to the maximum plastic zone radius, $d/r_{y,max}$. The yield stress gradient term can even

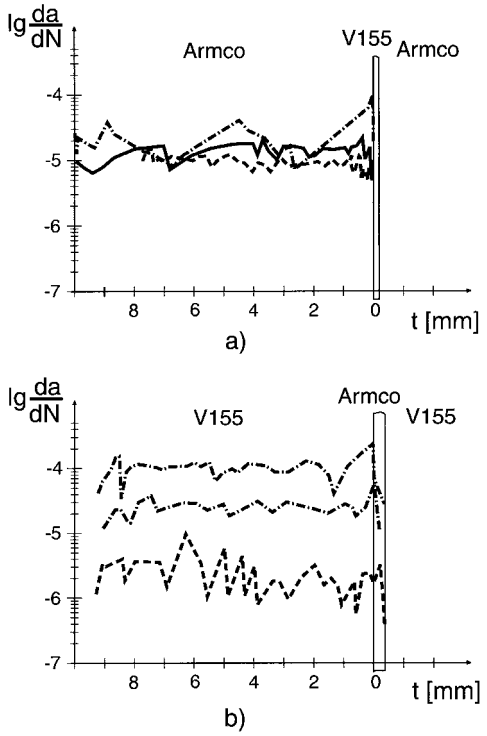

Fig. 15. Fatigue experiments by Pippan and Flechsig (1999). (a) Crack growth rate, da/dN, in Armco–iron against the distance, t, to a hard V155 steel interlayer. The cracks stop near the first interface. (b) Crack growth rate in V155 steel near a soft Armco–iron interlayer. The cracks stop near the second interface.

drop, if due to the increase in the plastic zone size the $d/r_{y,max}$-ratio falls clearly below 1. A similar observation will be made in layered materials, if $r_{y,max}$ becomes significantly larger than the periodicity of the material.

Another conclusion can be drawn: a gradient in the hydrostatic stress state will change the plastic strain energy of the plastic zone. Thus, a yield stress gradient term will be induced by a T-stress gradient, e.g., by a transition from plane strain to plane stress conditions near a free surface, or by a gradient in residual stresses.

4.5. The yield stress gradient effect in fatigue

It has been noted above that the ratio of the plastic zone radius to some microstructural length effects the size of the yield stress gradient effect. For instance, if in layered materials the plastic zone size is much larger than the periodicity of the material, the yield stress gradient term is negligible. Therefore, the yield stress gradient effect is in many cases more important in fatigue where the plastic zone sizes are much smaller than in monotonically loaded structures.

The behavior of fatigue cracks in materials with smooth yield stress gradients or in materials with interfaces or interlayers can be (qualitatively) predicted with our model: At a transition soft–hard, a positive cyclic yield stress gradient term diminishes the cyclic crack driving force; the crack growth rate decreases and the crack might even stop as has been seen in the experiments by Suresh et al. (1992). The

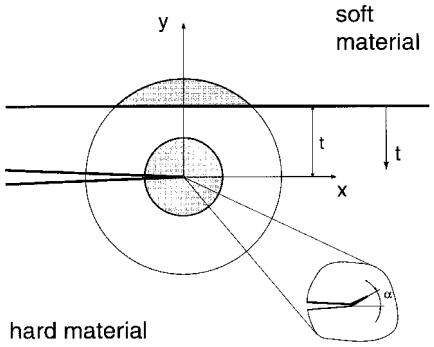

Fig. 16. Plastic zone for a crack in a hard material, parallel to an interface to a soft material. The crack will change its path and curve towards the interface.

positive effect of a soft Ni–5Al interlayer between a steel and the Cr_2O_3-coating on the S–N curve, which was reported in Suresh et al. (1993), finds its explanation in Section 3.3.4.

Pippan and Flechsig (1999) conducted experimental studies on the behavior of fatigue cracks near bimaterial interfaces and interlayers. The specimens, which were diffusion bonded under high pressure, consist of Armco iron ($\sigma_y = 141$ MPa) and a quenched and tempered ferritic steel V155 ($\sigma_y = 530$ MPa). The specimens were fatigued at constant stress intensity ranges, ΔK = 25, 18, and 10 MPa/m^2; the crack propagation rate was measured optically on both sides of the specimens. Hard–soft and soft–hard bimaterial transitions were studied, as well as Armco-interlayers in steel and steel interlayers in Armco iron. The thickness of the interlayers was varied. The predictions of the model fit to the experimental results: The fatigue crack slows down, stops and bifurcates into two (near-) interface cracks at a soft–hard bimaterial interface; the crack velocity increases near the interface at a hard–soft transition.

Both a steel interlayer in Armco iron and a soft Armco iron interlayer in steel prevent the crack from proceeding further into the specimen. In both cases, the crack bifurcates into two interface cracks. As it is predicted by the model, the crack stops at the first interface when a hard steel interlayer is embedded in Armco iron, see Fig. 15(a). It is worth to mention that the situation for ΔK = 25 MPa/m^2 is similar to those shown in Fig. 11: the ratio of the cyclic plastic zones in the two materials is approximately 1:10, and the thickness of the Steel V155 interlayer is a little bit smaller than the cyclic plastic zone radius in the base material.

For an Armco interlayer in steel, the crack stops in front of the second interface which has a soft–hard transition, Fig. 15(b).

4.6. Further implications of the yield stress gradient effect

4.6.1. Cracks parallel to interfaces

Imagine several specimens where a crack is growing parallel to an interface between a plastically soft and hard material. The specimens are otherwise identical (geometry, crack length, etc.), but the distance, t, between crack and interface is different. The plastic zone sizes in the two materials are denoted $r_{y,hard}$ and $r_{y,soft}$. Comparing the potential energy of the specimens at the same load, we will find that the specimens with the largest plastic zones, i.e., those with a crack in the soft material remote from the interface, have the smallest potential energy.

Now consider a specimen with a crack in the hard material, Fig. 16. We assume a meandering crack; the crack extension steps are sometimes inclined towards the interface, sometimes away from the interface. If t is larger than $r_{y,soft}$, the crack will always feel the same potential energy and it will steadily

grow at the same distance from the interface. For $t \leq r_{y,soft}$, the crack feels a smaller potential energy if the crack extension step is directed towards the interface. Due to the gradient dW_{pl}/dt, the crack driving force for a kinked crack with a kink angle α towards the interface is slightly larger than those for a kink with $-\alpha$. Therefore, the crack will change its path and curve towards the interface. For a perfect interface with a high interface toughness, the crack will cross the interface to reach the position of minimum potential energy at $t = -r_{y,soft}$. This is the equilibrium position for all initial cracks lying at $|t| \leq r_{y,soft}$.

In several papers, Tschegg and co-workers studied the behavior of cracks parallel to bimaterial interfaces (Tschegg et al., 1990, 1991; Tschegg et al., 1993; Tschegg et al., 1994). The bimaterials were produced by explosion cladding. Different material combinations were used: austenitic and ferritic steel, aluminium and ferritic steel, or copper and ferritic steel. Tests were made on 3-Point Bend specimens under monotonic (Tschegg et al., 1993; Tschegg et al., 1994) and cyclic loading (Tschegg et al., 1990, 1991). If the interface toughness was high enough, exactly the behavior was observed as has been described above, see Figs. 7 and 8 in Tschegg et al. (1994).

4.6.2. On the influence of the microstructure on the crack path

The results of Eq. (3) can be generalized to improve the understanding how microstructural features influence the microscopic behavior of cracks. Consider, instead of hard or soft interlayers, particles that have a high or low yield stress compared to the base material. When a crack comes near to the particles, the yield stress gradient effect will reduce or increase the local crack driving force. The effect will be significant when the particle size has the same order of magnitude as the plastic zone in the base material.

A high-strength second-phase particle is very often attended by a corona of high constraint around it. The gradient in hydrostatic stress in the base material around the particle will amplify the yield stress gradient effect, as has been described in Section 4.4. The primary reason for the amplification is that the effective radius of the particles for producing a yield stress gradient effect is increased.

When a crack is approaching a hard particle, the yield stress gradient term reduces the total crack driving force; when the crack leaves the particle or the high-constraint corona, the total crack driving force is enhanced. However, in many cases the crack will not go through the particle. A meandering crack that approaches the high-constraint corona below its center will feel a lower crack driving force for a kink with a positive kink angle, α, than for a kink with $-\alpha$. Hence, the crack will deviate from its original path and circumvent the particle. Analogously, a low-strength particle or a void will attract the crack.

In general, the Young's modulus of a particle will also differ from the matrix value. As has been noted in Section 2, the modulus gradient will induce an additional crack driving force component. The modulus gradient term has the same sign as the yield stress gradient term: it is negative for a transition compliant–stiff, and positive for a transition stiff–compliant. The total effect of particles on the local crack driving force results as an interaction of both the plasticity and the modulus gradient effect.

The yield stress gradient effect affects strongly the crack path in inhomogeneous elastic–plastic materials. The general rule, "A crack wants to propagate so that the total potential energy of the system becomes a minimum", seems to be equivalent to the more perceptive rule, "A crack wants to propagate so that the dissipated energy becomes a maximum".

5. Summary

In elastic–plastic materials, a plastic zone appears at the tip of a loaded crack. Whenever the plastic strain energy in the plastic zone changes in the direction of the crack extension, the crack driving force near the tip becomes different from the nominally applied far-field value. This effect is termed yield stress gradient effect. In this paper, an analytical model has been presented to quantify the effect for small-

scale yielding conditions. The model is based on global energy considerations. The effect of T-stresses and of plane strain or plane stress conditions can be taken into account.

It is demonstrated that in materials with a smooth gradient in yield stress an additional crack-driving force term appears, the yield stress gradient term, C_y. C_y is positive, i.e., it enhances the effective crack driving force when the yield stress decreases in crack growth direction. On the contrary, an increase of the yield stress induces a negative yield stress gradient term which diminishes the effective crack driving force. The size of C_y is proportional to the applied far-field crack driving force, the yield stress gradient and the plastic zone size.

A yield stress gradient term is also induced when in inhomogeneous materials the crack tip plastic zone interacts with interfaces that separate regions of different yield stresses. Analytical expressions for the yield stress gradient term near bimaterial interfaces and near interlayers have been developed. The evaluations show that bimaterial transitions from a hard to a soft material increase the crack driving force, soft–hard transitions decrease it. The size of the yield stress gradient term depends primarily on the ratio of the plastic zone sizes in the two materials. The predictions of the model agree well with the results of finite element computations by Sugimura et al. (1995). Experimental observations of the behavior of fatigue cracks near bimaterial interfaces between ferritic and austenitic steel (Suresh et al., 1992, 1993) and between steel and Armco iron (Pippan and Flechsig, 1999) can be qualitatively explained.

Both soft and hard interlayers can act as effective obstacles for cracks, provided that the interlayer thickness is of the order of the plastic zone radius of the softer material, or larger. For hard interlayers, the crack driving force has its minimum in front of the first interface; for soft interlayers, the minimum appears near the second interface. These predictions have been confirmed experimentally by Pippan and Flechsig (1999).

The derived expressions for C_y can be used to optimize functionally graded materials and interface and interlayer transitions in composites so that the fracture resistance increases. Further implications of the yield stress gradient effect for cracks parallel to interfaces and for the behavior of cracks near hard or soft particles have been discussed.

The yield stress gradient effect plays an important role for the fracture behavior in multiphase or composite materials, in functionally graded materials, as well as in materials with special surface treatments like nitrided or case-hardened steels, shot peened materials, or in ion implantation. Further applications are found in brazed or welded components, or in components where the yield stress changes due to steep temperature gradients.

Acknowledgements

This paper was written during a research visit in Professor Subra Suresh's laboratory at MIT. The author would like to thank Professor Suresh for many helpful discussions and for reviewing the manuscript. A partial funding of the research visit by the Austrian Academy of Sciences is acknowledged.

References

Bao, G., Wang, L., 1998. International Journal of Solids and Structures 35, 701–717.

Chen, W.-H., Chen, K.-T., Chiang, C.-R., 1988. On the applicability of J_{Ro} integral for perpendicular interface crack. Engineering Fracture Mechanics 30, 13–19.

Choi, H.J., 1996. Bonded dissimilar strips with a crack perpendicular to the functionally graded interface. International Journal of Solids and Structures 33, 4101–4117.

Cook, T.S., Erdogan, F., 1972. Stresses in bonded materials with a crack perpendicular to the interface. International Journal of Engineering Science 10, 667–696.

Delale, F., Erdogan, F., 1983. The crack problem for a nonhomogeneous plane. Journal of Applied Mechanics 50, 609–614.
Delale, F., Erdogan, F., 1988. On the mechanical modelling of the interfacial region in bonded half-planes. Journal of Applied Mechanics 55, 317–324.
Delfin, P., Gunnars, J., Ståhle, P., 1995. Effect of elastic mismatch on the growth of a crack initially terminated at an interface in elastic plastic bimaterials. Fatigue and Fracture of Engineering Materials and Structures 18, 1201–1212.
Erdogan, F., 1995. Fracture mechanics of functionally graded materials. Composites Engineering 5, 753–770.
Erdogan, F., Kaya, A.C., Joseph, P.F., 1991. The crack problem in bonded nonhomogeneous materials. Journal of Applied Mechanics 58, 410–418.
Erdogan, F., Wu, B.H., 1997. The surface crack problem for a plate with functionally graded properties. Journal of Applied Mechanics 64, 449–456.
Gu, P., Asaro, R.J., 1997a. International Journal of Solids and Structures 34, 1–17.
Gu, P., Asaro, R.J., 1997b. International Journal of Solids and Structures 34, 3085–3098.
He, M.-Y., Hutchinson, J.W., 1989. Crack deflection at an interface between dissimilar elastic materials. International Journal of Solids and Structures 25, 1053–1067.
He, M.Y., McMeeking, R.M., Zhang, N.T., 1992. Small scale yielding ata crack normal to the interface between an elastic and a yielding material. In: Materials Research Society Symposium Proceedings, vol. 239, pp. 585–590.
Honein, T., Herrmann, G., 1997. Conservation laws in nonhomogeneous plane elastostatics. Journal of the Mechanics and Physics of Solids 45, 789–805.
Hutchinson, J.W., 1968. Singular behavior at the end of a tensile crack tip in a hardening material. Journal of the Mechanics and Physics of Solids 16, 13–31.
Hutchinson, J.W., Suo, Z., 1992. Mixed mode cracking in layered materials. Advances in Applied Mechanics 29, 63–191.
Irwin, G.R., 1957. Analysis of stresses and strains near the end of a crack traversing a plate. Journal of Applied Mechanics 24, 361–364.
Irwin, G.R., 1961. Plastic zone near a crack and fracture toughness. In: Sagamore Research Conference Proceedings, vol. 4.
Kim, A.S., Suresh, S., Shih, C.F., 1997. Plasticity effects on fracture normal to interfaces with homogeneous and graded compositions. International Journal of Solids and Structures 34, 3415–3432.
Kumar, V., German, M.D., Shih, C.F., 1981. An Engineering Approach for Elastic–Plastic Fracture Analysis. Electric Power Research Institute, Palo Alto, CA EPRI-Report NP-1931.
Kolednik, O., Suresh, S., 1998. The influence of a yield strength gradient on the fracture resistance in FGMs. In: 5th International Symposium on Functionally Graded Materials (FGM '98). Trans Tech Publications, Zurich.
Larsson, S.G., Carlsson, A.J., 1973. Influence of non-singular stress terms and specimen geometry on small-scale yielding at crack tips in elastic–plastic materials. Journal of the Mechanics and Physics of Solids 21, 263–277.
Lee, W., Howard, J., Clegg, W.J., 1996. Growth of interface defects and its effect on crack deflection and toughening criteria. Acta Materialia 44, 3905–3922.
Martinez, D., Gupta, V., 1994. Energy criterion for crack deflection at an interface between two orthotropic media. Journal of the Mechanics and Physics of Solids 42, 1242–1271.
Pippan, R., Flechsig, K., 1999. Fatigue crack propagation behavior in the vicinity of an interface between materials with different yield stresses. Materials Science and Engineering (submitted for publication).
Pippan, R., Riemelmoser, F.O., Flechsig, K., 1998. The driving force on a crack approaching an interface of materials with different yield stresses: the effect of the interlayer thickness. In: Brebbia, C.A., Carpinteri, A. (Eds.), Damage and Fracture Mechanics — Computer Aided Assessment and Control. Computational Mechanics Publications, pp. 175–185.
Pippan, R., Riemelmoser, F.O., 1999. Fatigue of bimaterials. Investigation of the plastic mismatch in case of cracks perpendicular to the interface. Computational Materials Science (in press).
Rice, J.R., 1968a. Mathematical analysis in the mechanics of fracture. In: Liebowitz, H. (Ed.), Fracture, vol. 2. Academic Press, New York, pp. 191–311.
Rice, J.R., 1968b. A path independent integral and the approximate analysis of strain concentration by notches and cracks. Journal of Applied Mechanics 35, 379–386.
Rice, J.R., 1974. Limitations to the small scale yielding approximation for crack tip plasticity. Journal of the Mechanics and Physics of Solids 22, 17–26.
Rice, J.R., 1988. Elastic fracture mechanics concepts for interfacial cracks. Journal of Applied Mechanics 55, 98–103.
Rice, J.R., Rosengren, G.F., 1968. Journal of the Mechanics and Physics of Solids 16, 1–12.
Romeo, A., Ballarini, R., 1995. A crack very close to a bimaterial interface. Journal of Applied Mechanics 62, 614–619.
Romeo, A., Ballarini, R., 1997. A cohesive zone model for cracks terminating at a bimaterial interface. International Journal of Solids and Structures 34, 1307–1326.
Shih, C.F., 1991. Cracks on bimaterial interfaces: elasticity and plasticity aspects. Materials Science and Engineering A143, 77–90.
Stampfl, J., Scherer, S., Berchthaler, M., Gruber, M., Kolednik, O., 1996. Determination of the fracture toughness by automatic image processing. International Journal of Fracture 78, 35–44.

Stampfl, J., Kolednik, O., 1998. The separation of the fracture energy in metallic materials. International Journal of Fracture (in press).

Sugimura, Y., Lim, P.G., Shih, C.F., Suresh, S., 1995. Fracture normal to a bimaterial interface: effects of plasticity on crack-tip shielding and amplification. Acta Metallica Materialia 43, 1157–1169.

Suresh, S., Mortensen, A., 1998. Fundamentals of Functionally Graded Materials. University Press, Cambridge, UK.

Suresh, S., Sugimura, Y., Tschegg, E., 1992. The growth of a fatigue crack approaching a perpendicularly-oriented, bimaterial interface. Scripta Metallurgica 27, 1189–1194.

Suresh, S., Sugimura, Y., Ogawa, T., 1993. Fatigue cracking in materials with brittle surface coatings. Scripta Metallurgica 29, 237–242.

Tschegg, E.K., Kirchner, H.O.K., Kocak, M., 1990. Cracks at the ferrite–austenite interface. Acta Metallica Materialia 38, 469–478.

Tschegg, E.K., Kirchner, H.O.K., Schwalbe, K.-H., 1993. Cracks at interfaces of different cohesion. Acta Metallica Materialia 41, 2783–2790.

Tschegg, E.K., Kirchner, H.O.K., Kocak, M., 1991. Interfacial and subinterfacial cracks in the copper-ferrite system. Engineering Fracture Mechanics 39, 739–750.

Tschegg, E.K., Kirchner, H.O.K., Kocak, M., Zelezny, M.F., 1994. Subinterfacial fracture in bimaterial joints. In: Schwalbe, K.-H., Kocak, M. (Eds.), Mis-matching of Welds, ES1S17. Mechanical Engineering Publications, London, pp. 291–305.

Wang, T.C., Ståhle, P., 1998. Stress state in front of a crack perpendicular to bimaterial interface. Engineering Fracture Mechanics 59, 471–485.

Williams, M.L., 1959. The stresses around a fault or crack in dissimilar media. Bulletin of the Seismological Society of America 49, 199–204.

Zak, A.R., Williams, M.L., 1963. Crack point singularities at a bi-material interface. Journal of Applied Mechanics 30, 142–143.